Research Article

Qing Li and Fengzhou Fang*

Impacts of the gradient-index crystalline lens structure on its peripheral optical power profile

https://doi.org/10.1515/aot-2022-0003
Received January 19, 2022; accepted April 10, 2022;
published online May 2, 2022

Abstract: The crystalline lens makes an important contribution to the peripheral refraction of the human eye, which may affect the development and progression of myopia. However, little has been known about the peripheral optical features of the crystalline lens and its impacts on the peripheral ocular refraction. This study aims to investigate the relationship between the structural parameters of the crystalline lens and its peripheral power profile over a wide visual field. The peripheral power profile is defined with respect to the entrance and exit pupil centers along the chief rays. Analysis is performed by three-dimensional ray tracing through the gradient refractive index (GRIN) lens models built from measurement data. It has been found that the vergence of the wavefronts at the entrance and the exit pupil centers of the lens show an approximate linear correlation to each other for each field angle. The exponent parameters of the axial refractive index profile and the axial curvature profile, and the asphericity of the posterior lens surface are found to be the most influential parameters in the peripheral power profiles. The study also shows that there can be significantly different, sometimes unrealistic, power profiles in the homogeneous lens model compared with its corresponding GRIN model with the same external geometry. The theoretical findings on the peripheral lens properties provide a new perspective for both wide-field eye modelling and the design of intraocular lenses to achieve normal peripheral vision.

***Corresponding author: Fengzhou Fang**, Centre of Micro/Nano Manufacturing Technology (MNMT-Dublin), University College Dublin, Dublin 4, Ireland; and State Key Laboratory of Precision Measuring Technology and Instruments, Laboratory of Micro/Nano Manufacturing Technology (MNMT), Tianjin University, Tianjin 300072, China, E-mail: fengzhou.fang@ucd.ie. https://orcid.org/0000-0002-8716-5988
Qing Li, Centre of Micro/Nano Manufacturing Technology (MNMT-Dublin), University College Dublin, Dublin 4, Ireland

Keywords: crystalline lens; peripheral defocus; peripheral optical power.

1 Introduction

In the past decades, the peripheral refractions of the human eye have attracted much attention due to its potential impacts on the progression of myopia [1–3]. As the most complex ocular component, the crystalline lens is a major contributor to the profiles of the peripheral refractions. The lens grows rapidly before adulthood with changes in both structural and optical properties [4, 5]. Meanwhile, the lens structure changes dynamically during accommodation for near vision, which is also a potential factor for the development of myopia [6, 7]. These changes in the lens structure can affect the peripheral ocular refractions and thus may influence the progression of myopia. Therefore, to understand the optical mechanism of myopia, it is fundamental to understand how the lens structure contributes to the distribution of the peripheral refractions of the human eye.

Very few studies have focused on the peripheral optical features of the crystalline lens. Up until now, only one experimental study was found to have measured the peripheral defocus profile of the *in vitro* human lenses [8], but the interpretations of the measured data lacked a further understanding in terms of their relationship with the peripheral ocular refractions. Meanwhile, most of the previous crystalline lens models were built based on a limited number of parameters [9–13]. This results in the restricted capability of the lens model in predicting the peripheral ocular features while maintaining a realistic anatomic structure. Consequently, little is known about the relationship between the lens structure and its peripheral optical properties.

As a further step from our previous work on the physiology-like crystalline lens (PCL) model [14] that was built to reproduce the peripheral physiologic structure of the natural lens, this study aims to investigate the relationship between the lens structure and its peripheral power profile, identifying the impacts of the external lens geometry and the internal gradient refractive index (GRIN) structure. This work provides a new perspective for the wide-field eye modelling and the design of intraocular lenses for a natural peripheral visual quality.

2 Theoretical approaches

2.1 Establishment of the lens models

The lens models analysed in this study were developed from the PCL model [14], with the posterior external surface patches replaced by one fourth-order polynomial surface to achieve continuity of innumerable derivatives across the entire surface. The modification is based on the fact that a wide zone of the posterior lens surface covers the pathway of the rays for the peripheral visual field. Continuity of the surface geometry ensures the reproduction of realistic peripheral power profiles. As shown in Figure 1, the external lens surface is represented by

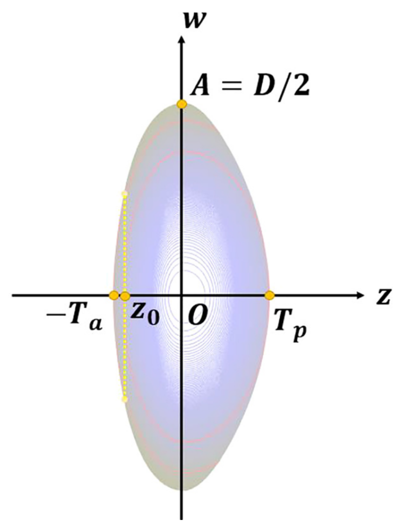

Figure 1: Diagram for the modified PCL model with the Z axis pointing towards the retina.

$$w^2 = x^2 + y^2 = \begin{cases} 2(z+T_a)R_a - (1+Q_a)(z+T_a)^2, & -T_a \le z \le z_0 \\ C_{1a}z^3 + C_{2a}z^2 + A^2, & z_0 \le z \le 0 \\ 2(-z+T_p)R_p - (1+Q_p)(-z+T_p)^2 + B_{3p}(-z+T_p)^3 + B_{4p}(-z+T_p)^4, & 0 \le z \le T_p \end{cases} \quad (1)$$

where C_{1a}, C_{2a}, B_{3p}, and B_{4p} are derived by the boundary conditions of smooth (first derivative) connection with the adjacent patch. The equations for the internal iso-indicial surfaces are

$$\begin{cases} \dfrac{z^2}{\left(T_a \times \sqrt[p]{\frac{n_{s\_e}-n_0}{n_{s\_a}-n_0}} \times \gamma\right)^2} + \dfrac{x^2+y^2}{(D/2)^2\gamma^{q+1}} = 1, & z \le 0 \\ \dfrac{z^2}{\left((T-T_a) \times \sqrt[p]{\frac{n_{s\_e}-n_0}{n_{s\_p}-n_0}} \times \gamma\right)^2} + \dfrac{x^2+y^2}{(D/2)^2\gamma^{q+1}} = 1, & z \ge 0 \end{cases}, \text{ where } \gamma = \sqrt[p]{\frac{n-n_0}{n_{s\_e}-n_0}}. \quad (2)$$

The meanings and settings of the lens parameters in Eqs. (1) and (2) can be seen in Table 1. All the values were determined from the measurement data on the human eye. The optical contribution of each parameter is analysed separately within the 'range for investigation' as shown in Table 1, based on the variation among the population.

2.2 Definition of the peripheral lens power

In Gaussian optical theory, the optical power Φ is defined for the paraxial region along the optical axis of a rotationally symmetric optical system,

$$\Phi = \frac{n_2}{l_{P2}} - \frac{n_1}{l_{P1}}, \quad (3)$$

where n_1 and n_2 are the refractive indices for the object and image space, respectively, l_{P1} is the axial distance from the primary principal point (P1) to the object point, and l_{P2} is the axial distance from the secondary principal point (P2) to the image point. Based on Eq. (3), Φ can be interpreted as the vergence of the emergent wavefront at P2 subtracted by the vergence of the incident wavefront at P1. The difference in the vergence of the wavefronts at these two points is always constant within the paraxial region. However, the paraxial condition can be rarely met in the peripheral visual field of the lens. Thus, new definitions need to be developed for the peripheral optical power.

To understand the contribution of the lens to the peripheral ocular refractions, the definition of the peripheral optical power of the lens should have a direct relationship with the peripheral refraction of the eye, which is defined along the chief rays passing through the pupil center. Therefore, the peripheral optical power of the lens—here named as the 'pupil power', Φ_{pupil}—is defined as the difference in the wavefront vergence between the exit and entrance pupil centers. As shown in Figure 2, for a chief ray in the aqueous humor,

$$\Phi_{pupil}(\theta_{aq}, v_{in}) = v_{out}(\theta_{aq}, v_{in}) - v_{in}, \quad (4)$$

where θ_{aq} is the angular interval between the chief ray and the lens axis; v_{out} and v_{in}, respectively, represent the vergence of the output and input wavefronts at either the exit pupil center or the entrance pupil center, depending on the direction of light propagation. In the definition of the ocular aberrations, the rays are traced from the vitreous

Table 1: Lens parameters[a] for the physiology-like crystalline lens model of age 11 years and the range for investigation.

Parameter	Meaning of the parameter	Value	Range for investigation	Source of data[c]
R_a (mm)	Radius of curvature at the anterior lens vertex	11.580	11–15	Mutti et al. [4]
R_p (mm)	Radius of curvature at the posterior lens vertex	6.303	6–8.5	Mutti et al. [4]
Q_a	Asphericity of the anterior external surface	4.6×10^{-4}	−22 to 5	Ishii et al. [15], Dubbelman et al. [16]
Q_p	Asphericity of the posterior external surface	2.49×10^{-4}	−15 to 3	Ishii et al. [15], Dubbelman and Van der Heijde [16]
T (mm)	Axial lens thickness	3.421	2.9–4.1	Mutti et al. [4]
T_a/T	Ratio of axial thicknesses between the anterior lens section and the total lens thickness	0.45	0.4–0.52	Martinez-Enriquez et al. [17], Ishii et al. [15]
D	Lens diameter	8.574	8–8.8	Ishii et al. [15]
n_0[b]	Refractive index at the lens center	1.4012	1.4–1.41	Khan et al. [18]
n_{s_a}[b]	Refractive index at the anterior lens vertex	1.3663	1.36–1.38	Khan et al. [18]
n_{s_p}[b]	Refractive index at the posterior lens vertex	1.3801	1.376–1.382	Khan et al. [18]
n_{s_e}[b]	Refractive index at the equatorial edge	1.3560	1.34–1.362	Khan et al. [18]
p	Exponent parameter for the axial index profile	3.3120	2–4.2	Khan et al. [18]
q	Exponent parameter for the axial curvature profile	1.494	1.2–2.2	Set to fit the paraxial lens power measured by Mutti et al. [4]
θ_a (°)	Subtended angle to the lens center of the conic zone on the anterior external surface	120	Not available	Set to cover the optical zone

[a]Elaboration of the parameters can be seen in the article by Li and Fang [14]. [b]All the refractive index parameters are referenced to the wavelength of 589 nm. [c]Source of data for the lens parameters is based on the average and range of data measured in the population, which were applied in this study for investigating their impacts on the peripheral lens power.

humor throughout the lens, thus v_{out} and v_{in} correspond to the wavefronts at the iris center (C_{aq}) and its conjugate point in the vitreous humor (C_{vi}), respectively. It is expected that Φ_{pupil} may vary with v_{in}; hence Φ_{pupil} is formulated as a function of both θ_{aq} and v_{in}.

The vergence of a wavefront is essentially the multiplication of the refractive index and the local curvature of the wavefront surface. In three-dimensional ray tracing, the wavefront surface is often not rotationally symmetric. As defined in differential geometry, the curvature at a point on the surface can be described by two local principal curvature values—the maximum and minimum curvature (κ_{max} and κ_{min}) along the two perpendicular directions [19]. Hence, the vergence of a wavefront also has two components, namely the spherical equivalent vergence (v_{SE}) and the plus cylinder vergence (v_{Cyl}), as shown below:

$$v_{SE} = n_{wave} \cdot \left(\frac{\kappa_{max} + \kappa_{min}}{2}\right), \tag{5.a}$$

$$v_{Cyl} = n_{wave} \cdot (\kappa_{max} - \kappa_{min}), \tag{5.b}$$

where n_{wave} is the refractive index of the medium for the wavefront. Similarly, Φ_{pupil} can be divided into two components—the spherical equivalent pupil power ($\Phi_{pupil-SE}$) and the plus cylinder pupil power ($\Phi_{pupil-Cyl}$), which are here defined as

$$\Phi_{pupil-SE} = v_{out-SE} - v_{in-SE}, \tag{6.a}$$

$$\Phi_{pupil-Cyl} = v_{out-Cyl} - v_{in-Cyl} \tag{6.b}$$

In the definition of the ocular aberrations, the input wavefront at C_{vi} is emitted from the point on the retina and is thus always spherical. Hence, $v_{in-Cyl} = 0$ and $\Phi_{pupil-Cyl}$ is essentially the plus cylinder vergence of the wavefront emerged at C_{aq}. It should be mentioned that the sign of v_{Cyl} is

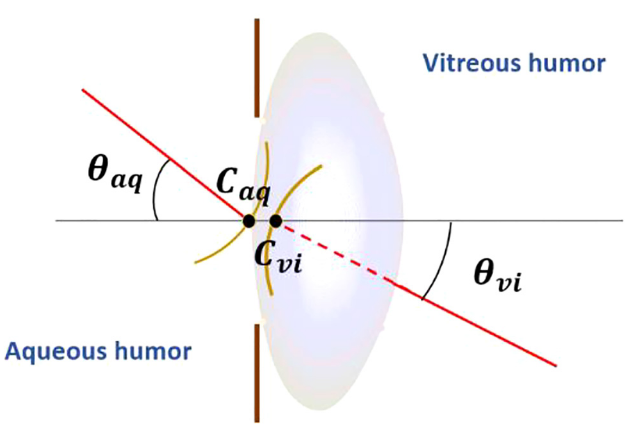

Figure 2: Diagram for defining the peripheral pupil power of the lens model along a chief ray (the red line) passing through the entrance and exit pupil centers C_{aq} and C_{vi}.

always positive, while the sign of v_{SE} follows the convention that a positive value corresponds to a converging wavefront.

2.3 Optical analysis procedure

In this study, the peripheral power profiles of the lens models as defined in Table 1 were obtained by three-dimensional ray tracing through a set of self-developed MATLAB programs. The detailed procedure is listed as follows.

(1) Finding C_{vi} of the lens model

In this study, C_{aq} is assumed to coincide with the anterior lens vertex. By tracing rays in the aqueous humor entering the lens that all pass through C_{aq}, the wavefront emerged out of the posterior lens surface can be derived as a series of points on the rays with the same optical path length from C_{aq}. The exit pupil center C_{vi} is then computed as the center of the sphere-fit to this wavefront.

(2) Locating the chief rays

For a given set of field angles θ_{aq}, the chief rays can be determined by ray tracing throughout the lens from the aqueous humor to the vitreous humor.

(3) Obtaining the relationship between Φ_{pupil} and v_{in-SE} for each field angle

Along the sections of the chief rays in the vitreous humor, a set of object points were located by a predefined set of v_{in-SE}, which determine the distances from C_{vi} with the given refractive index of the vitreous humor. Then, three-dimensional ray tracing was performed for each object point separately to obtain the wavefront emerged out of the anterior lens surface at C_{aq}. The wavefront was fitted to the Zernike polynomials up to the 6th order. The vergence parameters—v_{out-SE} and $v_{out-Cyl}$—of the emerging wavefront in the aqueous humor with the refractive index of n_{aq} were then calculated based on differential geometry and the power vector notation, as [20, 21]

$$v_{out-SE} = \frac{1}{R^2} \cdot \left(4\sqrt{3}\,c_2^0 - 12\sqrt{5}\,c_4^0 + 24\sqrt{7}\,c_6^0\right) \cdot n_{aq}, \quad (7.a)$$

$$v_{out-Cyl} = 2\sqrt{J_0^2 + J_{45}^2}, \quad (7.b)$$

$$J_0 = -\frac{1}{R^2}\left(2\sqrt{6}\,c_2^2 - 6\sqrt{10}\,c_4^2 + 12\sqrt{14}\,c_6^2\right) \cdot n_{aq}, \quad (7.c)$$

$$J_{45} = -\frac{1}{R^2}\left(2\sqrt{6}\,c_2^{-2} - 6\sqrt{10}\,c_4^{-2} + 12\sqrt{14}\,c_6^{-2}\right) \cdot n_{aq} \quad (7.d)$$

Here R is the semi-diameter of the wavefront; c_n^m are the Zernike coefficients; J_0 and J_{45} are the horizontal/vertical and the oblique power vectors of astigmatism in the power notation, respectively [20]. Note that Eq. (7.b) for $v_{out-Cyl}$ was derived in a similar way to the derivation of the plus cylinder power of the wavefront refraction of the human eye [20, 22]. In this study, the discussion of the crystalline lens is focused on a rotationally symmetric structure. For the ease of formulation, the peripheral lens power is analysed along the vertical meridian, in which case

$$v_{out-Cyl} = 2|J_0| \quad (8)$$

As shown in the section below, a mathematical pattern can be easily observed between J_0 and v_{in}, because there is no restriction on the sign of J_0. Thus, the trendlines of J_0 with respect to v_{in-SE} and θ_{aq} were calculated first, while $\Phi_{pupil-Cyl}$ can be derived afterwards by Eq. (8).

For all the calculations involved in this study, the wavefront diameter is set as 3 mm and the GRIN structure of the lens model is approximated by 200 iso-indicial layers. The refractive indices of the aqueous humor and the vitreous humor are set as 1.333. Around 5000 rays are traced throughout the lens. The boundary of the ray bundle is set wide enough so that the 1.5 mm-radius entrance pupil can be fully covered by the rays even at the most peripheral field angle.

3 Results

3.1 Evaluation of the lens pupil power

Based on the method described above, the peripheral lens power profile was computed on the 11-year-old lens model defined in Table 1. C_{vi} was calculated at 0.043 mm behind C_{aq} along the lens axis, suggesting that the iris center and its conjugate point almost coincide with each other. Meanwhile, it has been found that θ_{vi} is very close to θ_{aq} for each chief ray, as can be seen in Figure 3. Interestingly, θ_{vi} is approximately linear to θ_{aq} with the slope of 0.95. The R-squared value for the linear fit is 0.9998.

The changes in the lens pupil power with respect to the absolute value of v_{in-SE} are shown in Figure 4. All the trendlines appear approximately linear, which reveals a unique feature of the lens that can be applied to formulate the lens power. The maximum deviation of the linear fit to the relationship between $\Phi_{pupil-SE}$ and v_{in-SE} is below 0.025 D, while the maximum deviation for the linear fit between J_0 and v_{in-SE} is below 0.015 D. Moreover, both

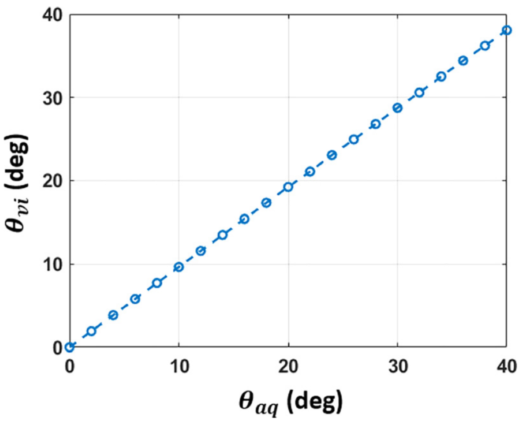

Figure 3: The change in the vitreous field angle θ_{vi} with respect to the aqueous field angle θ_{aq} for the chief rays.

$\Phi_{pupil-SE}$ and J_0 tend to decrease with larger magnitude of v_{in-SE} for the peripheral visual field. Meanwhile, for the same value of v_{in-SE}, both $\Phi_{pupil-SE}$ and $\Phi_{pupil-Cyl}$ tend to be larger for the more peripheral field, and the steepness of the trendlines increases with larger eccentricity. This indicates that the peripheral pupil power is more sensitive to v_{in-SE} of larger eccentricity.

3.2 Impacts of the lens structure

To understand how the structural features of the lens affect its peripheral power profile, 13 major lens parameters were investigated within the intervals measured on the population as listed in Table 1. In addition, the role of the gradient index distribution in the power profiles was also analysed, by comparing each lens model with its corresponding homogeneous model having the same external geometry. The refractive index of the homogeneous model is the equivalent refractive index (n_{eq}) of the GRIN model, which is computed by its paraxial optical power:

$$P_{paraxial-GRIN} = \frac{n_{eq} - n_{aq}}{R_a} + \frac{n_{vi} - n_{eq}}{R_p} - \frac{T}{n_{eq}} \cdot \frac{n_{eq} - n_{aq}}{R_a} \cdot \frac{n_{vi} - n_{eq}}{R_p} \quad (9)$$

To understand the situation in the eye, the peripheral lens power profile was analysed within a test eye model defined by a spherical retinal contour with a radius of curvature of 12 mm and an axial distance of 19 mm from C_{vi}. Since C_{vi} is quite close to the anterior lens vertex for all the lens models, the vitreous chamber depth is around 15–16 mm, which is within the range measured on children [23]. This leads to the value of v_{in-SE} decreasing from around −70 D at the central field to −81 D at the most peripheral visual field ($\theta_{vi} = 40°$).

The results for Qp are displayed in Figure 5. For most peripheral field locations of the GRIN models, both $\Phi_{pupil-SE}$ and $\Phi_{pupil-Cyl}$ increase with eccentricity and tend to be larger with higher Qp. The trendlines of $\Phi_{pupil-Cyl}$, in contrast, show a steeper increase with lower values of Qp at θ_{aq} >33°. In contrast, a reduction in both $\Phi_{pupil-SE}$ and

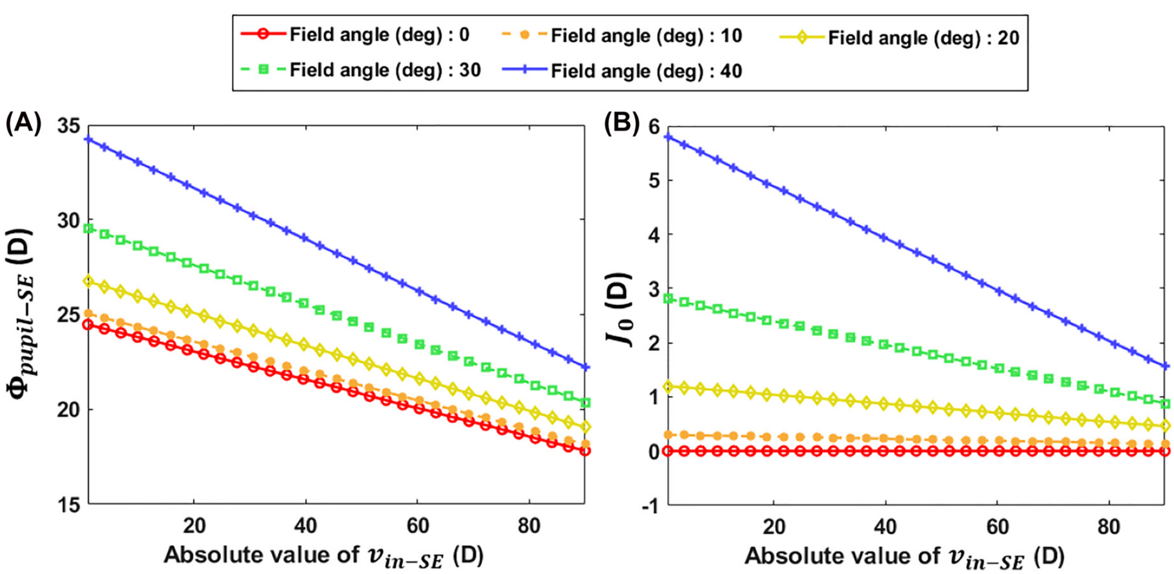

Figure 4: Change of $\Phi_{pupil-SE}$ (A) and J_0 (B) with respect to the absolute value of v_{in-SE}.

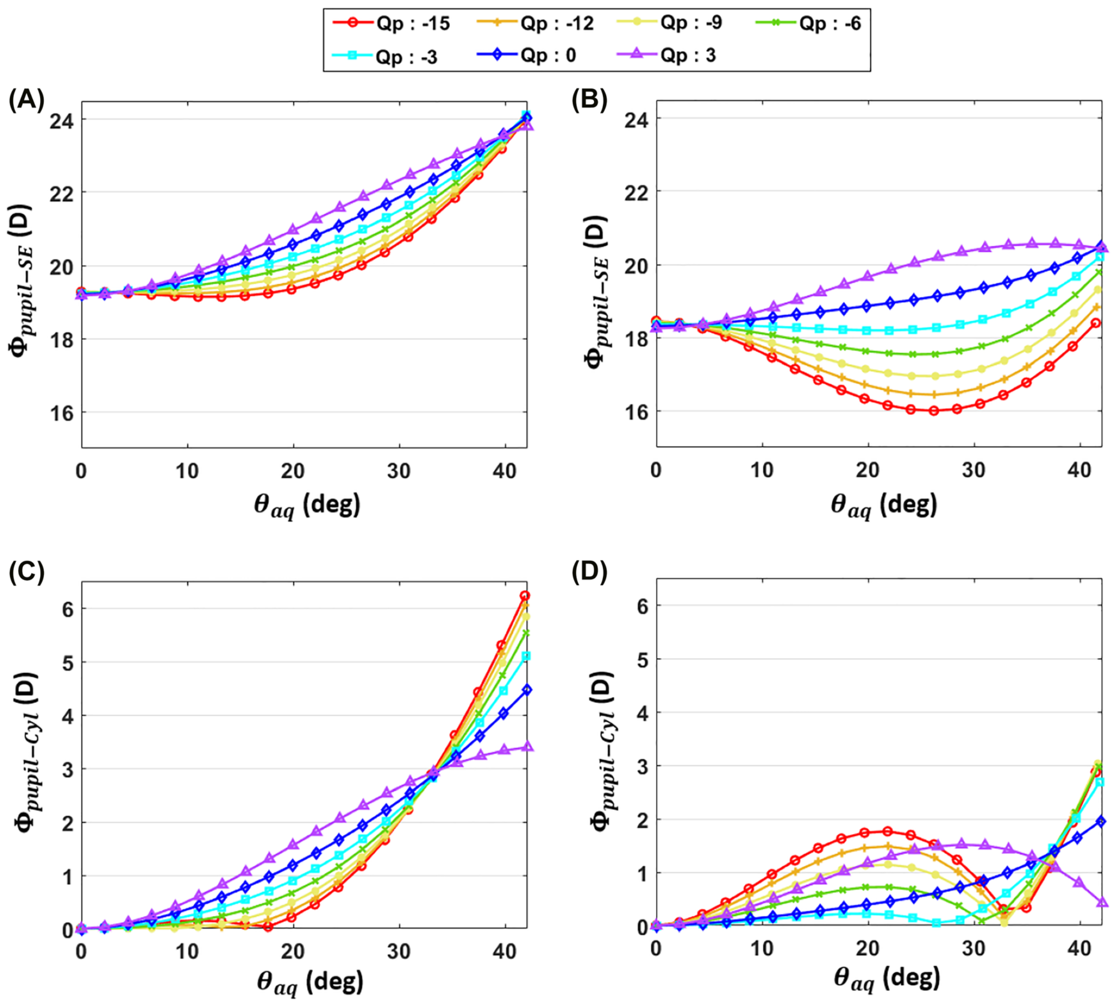

Figure 5: Peripheral power profiles of the 11-year lens model calculated in the test eye model with different values of *Qp*, including: (1) $\Phi_{pupil-SE}$ for the gradient refractive index (GRIN) (A) and homogeneous (B) models; (2) $\Phi_{pupil-Cyl}$ for the GRIN (C) and homogeneous (D) models.

$\Phi_{pupil-Cyl}$ with larger value of θ_{aq} can be observed in certain field ranges of the homogeneous models, and this pattern is more evident for the lower values of *Qp*. Comparison between the GRIN and the homogeneous models indicates that GRIN structure (1) contributes positively to the peripheral profile of $\Phi_{pupil-SE}$ and (2) induces opposite values of J_0 compared with the external geometry. These results suggest that having a realistic paraxial optical power alone does not ensure the lens model to have a realistic peripheral power profile.

The peripheral power profiles for the other lens parameters were also analysed by the same procedure. Overall, the distance between C_{vi} and C_{aq} is less than 0.06 mm, as can be seen in Figure 6(A). Meanwhile, θ_{vi} is approximately linear to θ_{aq}, with the value of θ_{vi}/θ_{aq} between 0.94 and 0.96 (Figure 6(B)). These results show that, very interestingly, the sections of the chief rays in the aqueous and vitreous humor are almost collinear to each other.

At around 25° of θ_{aq} in the test eye model, the change in the relative $\Phi_{pupil-SE}$ (peripheral value of $\Phi_{pupil-SE}$ minus the central value of $\Phi_{pupil-SE}$) with respect to the investigated range of the GRIN lens parameters (as stated in Table 1) are shown in Figure 7. As expected, the value of *Qa* does not influence the peripheral lens power. For the investigated range of each parameter, the exponent parameters *p* and *q* have the largest effects on the peripheral lens power, followed by *Qp* and n_{s_e}. Furthermore, it can be seen that the increases in *q*, n_{s_e}, *Ra* and *D* are associated with a decrease in the relative $\Phi_{pupil-SE}$, in contrast with the other lens parameters that are positively correlated with the relative $\Phi_{pupil-SE}$.

The results for $\Phi_{pupil-Cyl}$ can be seen in Figure 8. Similarly, the variation of $\Phi_{pupil-Cyl}$ is the largest for the

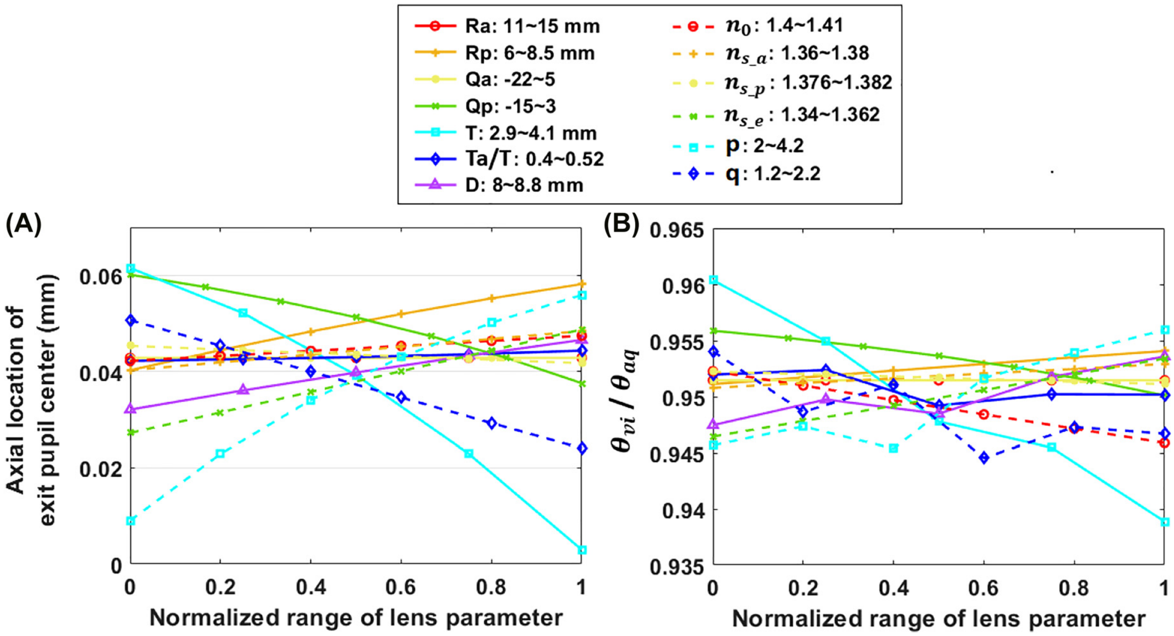

Figure 6: Trendlines of the distance between C_{aq} and C_{vi} (A) and the field ratio θ_{vi}/θ_{aq} (B) with respect to the normalised range of the lens parameter for all the investigated gradient refractive index lens models.

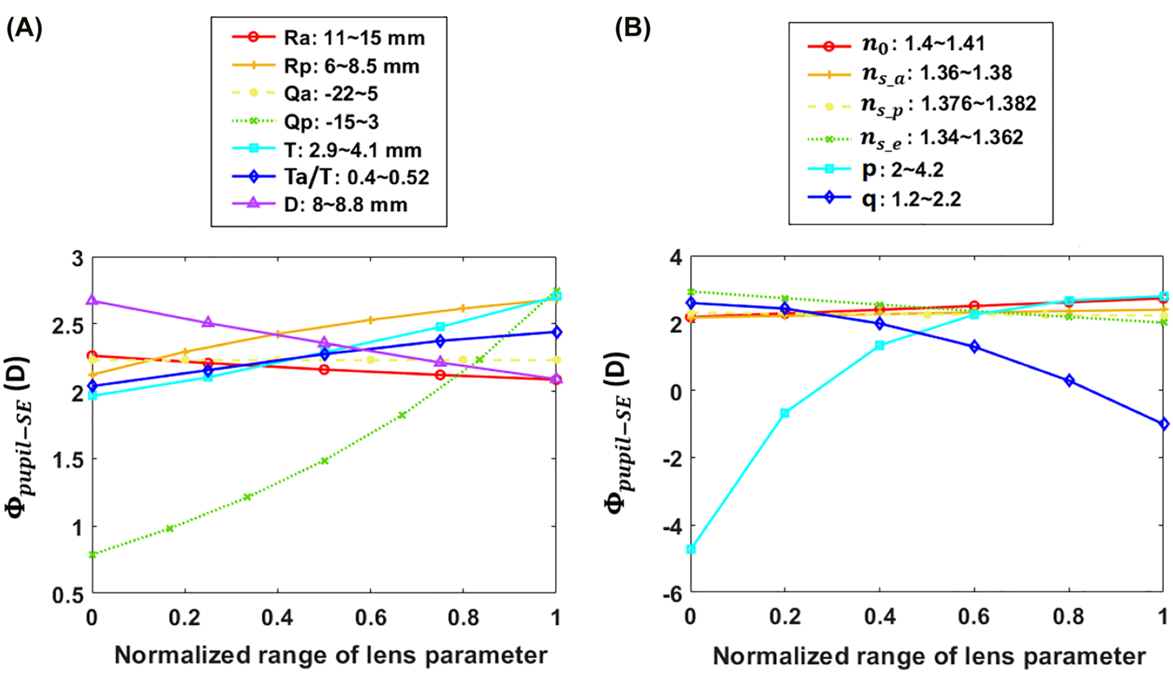

Figure 7: Change of the relative $\Phi_{pupil-SE}$ at around 25° of θ_{aq} with respect to the gradient refractive index (GRIN) lens parameters related to the external lens geometry (A) and the GRIN distribution (B).

investigated intervals of p and q, while the trendlines of the other lens parameters present a similar pattern to the trendlines of the relative $\Phi_{pupil-SE}$. Namely, a larger value of the relative $\Phi_{pupil-SE}$ is often associated with a larger value of $\Phi_{pupil-Cyl}$ regardless of the variations in the lens structure.

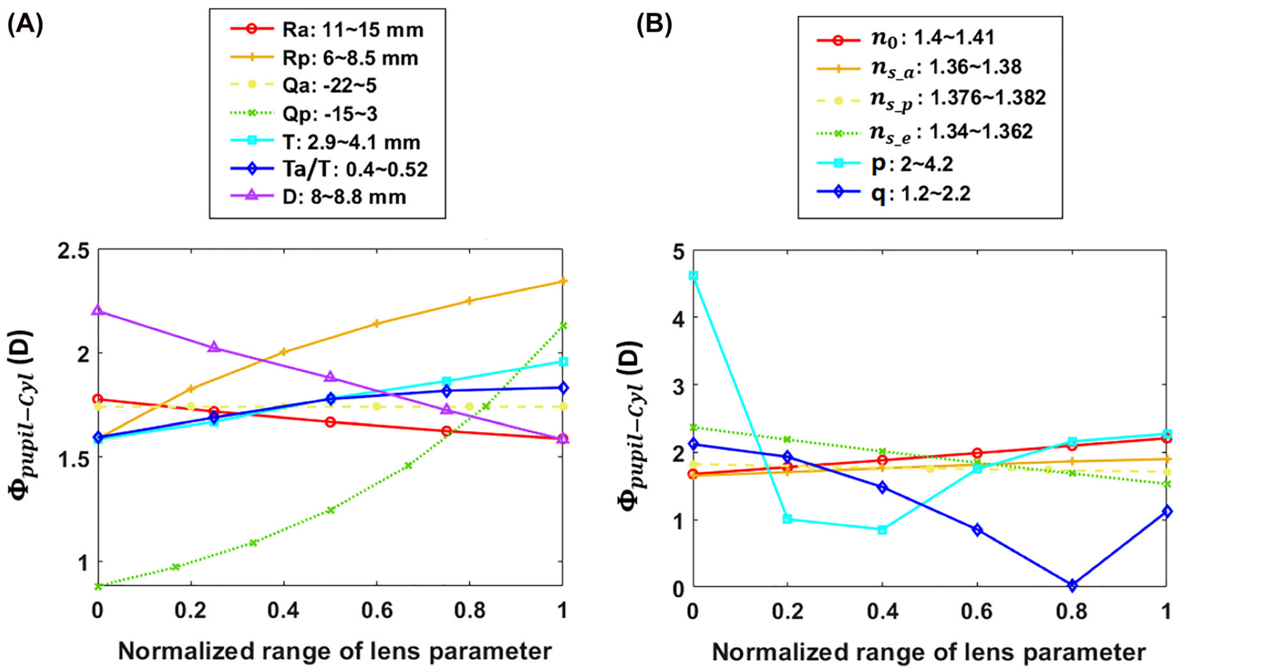

Figure 8: Change of $\Phi_{pupil-Cyl}$ at around 25° of θ_{aq} with respect to the lens parameters related to the external lens geometry (A) and the GRIN distribution (B).

4 Discussion

This study proposed a new way of describing the peripheral optical power of the crystalline lens—as the lens-induced change in the wavefront vergence between C_{aq} and C_{vi} along the chief rays. In this way, the contribution of the ocular components (lens, cornea and retina) to the peripheral refraction of the eye can be described separately and quantitatively with mathematical rigor. The ocular refraction is often equivalent to the vergence of the wavefront at the entrance pupil center of the eye, which is also the conjugate point of C_{aq} in the air. The wavefront has to be emitted from the point on the retina and propagates along the chief ray throughout the eye. Accordingly, the contribution from the retina can be represented by the vergence of the wavefront at C_{vi}, while the impact of the cornea and its location relative to the lens can be defined as the difference in the wavefront vergence between C_{aq} and the entrance pupil center of the eye.

As found by ray tracing through all the investigated lens models, the peripheral lens power (in terms of both $\Phi_{pupil-SE}$ and J_0) at the same visual field presents a highly linear correlation with the wavefront vergence at C_{vi} for all the field angles. Due to the complexity of the GRIN structure, an analytical explanation of this phenomenon cannot be easily derived. However, calculations of all the lens models show that C_{vi} is close to C_{aq} and θ_{aq} is close to θ_{vi} for the same chief ray. These findings indicate that the chief rays on both sides of the lens model are almost collinear to each other—having the feature of the optical axis defined in the paraxial optics. In the paraxial optical theory, the wavefront vergence at two conjugated points on the optical axis are always linear to each other [24], which could partially explain the linear relationship between $\Phi_{pupil-SE}$ and v_{in-SE}.

The proposed approach for analysing the peripheral lens power was then applied to evaluate the contribution of each lens structural feature within the range measured on the population. In this study, 13 lens parameters were examined based on a 11-year-old lens model constructed from measurement data. In particular, we found that the asphericity of the posterior lens surface plays a significant role in the power profile. This finding is helpful for wide-field eye modelling. Since Qp has nearly no impacts on the paraxial lens power, it can be adjusted to reproduce the targeted peripheral refraction profile. Furthermore, this study shows that the peripheral lens power changes the most with the variation of the exponent parameters for the axial index profile (p) and the curvature profile (q) within the examined interval, followed by Qp and n_{s_e}. These parameters should be given special attention in the construction of the accommodative eye models that aim for reproducing the measured change in the peripheral ocular refraction during accommodation.

The role of the GRIN structure as a whole has been investigated by comparing the GRIN and the homogeneous models of the same external geometry. Although both types of the lenses share the same value of the paraxial optical power, there can be large deviations in the peripheral optical profiles. Our analysis has shown that for lower values of Qp, negative correlations of $\Phi_{pupil-SE}$ and $\Phi_{pupil-Cyl}$ with respect to θ_{aq} are present in the homogeneous models, which are very rare for the GRIN models. This finding is especially helpful for building the physical eye models, where the crystalline lens is often modelled by a homogeneous lens. To achieve a realistic distribution of the peripheral refraction, the external geometry of the lens model should be manually modified rather than following the external geometry measured on the real lenses.

One limitation of this study is the assumption of a rotationally symmetric lens model, while studies have found some degree of the axial astigmatism in the human lens [25]. In such case, the wavefronts propagating along most of the peripheral chief rays will be distorted due to the torsion in the refracting surfaces. Moreover, the iris center is assumed to locate at the anterior lens vertex, while a slight decentration of the iris center with respect to the lens can exist in many eyes and during pupil constriction. Although these situations are insignificant in most eyes and thus ignored in many eye models, more measurement data of the peripheral optical and structural features of the human lens are needed to develop a further understanding.

5 Conclusions

This study proposed a new method for describing the peripheral optical power profiles of the crystalline lens model for the entire visual field. Based on this method, the relationship between the lens structure and its peripheral power profile was systematically investigated on a series of lens models constructed from measurement data. It has been found that the vergence of the wavefronts at the entrance and the exit pupil centers of the lens shows an almost linear correlation to each other for each field location. This can be partly explained by the high degree of collinearity between the sections of the chief rays in the vitreous and the aqueous humor as found in all the lenses. Among the 13 lens parameters, p, q, Qp, and n_{s_e} were found to have the largest impacts on the peripheral power profiles. The study also shows that there can be significantly different, sometimes unrealistic, power profiles in the homogeneous lens model compared with its corresponding GRIN model with the same external geometry. These findings can be helpful for building eye models and the design of intraocular lenses that aim to reproduce the peripheral ocular refraction profiles with high accuracy and efficiency.

Author contributions: All the authors have accepted responsibility for the entire content of this submitted manuscript and approved submission.
Research funding: The authors would like to thank the financial support from Science Foundation Ireland under Grant number (15/RP/B3208), and the State Administration of Foreign Experts Affairs and the Ministry of Education of China (No. B07014).
Conflict of interest statement: The authors declare that they have no known competing financial interests or personal relationships that could have appeared to influence the work reported in this paper.

References

[1] J. Wallman, and J. Winawer, “Homeostasis of eye growth and the question of myopia,” *Neuron*, vol. 43, pp. 447–468, 2004.
[2] E. L. Smith, R. Ramamirtham, Y. Qiao-Grider, et al., “Effects of foveal ablation on emmetropization and form-deprivation myopia,” *Investig. Ophthalmol. Vis. Sci.*, vol. 48, pp. 3914–3922, 2007.
[3] E. L. Smith III, L.-F. Hung, and J. Huang, “Relative peripheral hyperopic defocus alters central refractive development in infant monkeys,” *Vision Res.*, vol. 49, pp. 2386–2392, 2009.
[4] D. O. Mutti, K. Zadnik, R. E. Fusaro, N. E. Friedman, R. I. Sholtz, and A. J. Adams, “Optical and structural development of the crystalline lens in childhood,” *Invest. Ophthalmol. Vis. Sci.*, vol. 39, 120–133, 1998.
[5] J. Rozema, S. Dankert, R. Iribarren, C. Lanca, and S.-M. Saw, “Axial growth and lens power loss at myopia onset in Singaporean children,” *Investig. Ophthalmol. Vis. Sci.*, vol. 60, pp. 3091–3099, 2019.
[6] J. M. Ip, S.-M. Saw, K. A. Rose, et al., “Role of near work in myopia: findings in a sample of Australian school children,” *Invest. Ophthalmol. Vis. Sci.*, vol. 49, pp. 2903–2910, 2008.
[7] H.-M. Huang, D. S.-T. Chang, and P.-C. Wu, “The association between near work activities and myopia in children—a systematic review and meta-analysis,” *PLoS One*, vol. 10, 2015, Art no. e0140419.
[8] B. M. Heilman, A. Mohamed, M. Ruggeri, et al., “Age-dependence of the peripheral defocus of the isolated human crystalline lens,” *Invest. Ophthalmol. Vis. Sci.*, vol. 62, pp. 15, 2021.
[9] R. Navarro, “Adaptive model of the aging emmetropic eye and its changes with accommodation,” *J. Vis.*, vol. 14, p. 21, 2014.
[10] A. V. Goncharov, and C. Dainty, “Wide-field schematic eye models with gradient-index lens,” *J. Opt. Soc. Am. A*, vol. 24, pp. 2157–2174, 2007.

[11] M. Bahrami, and A. V. Goncharov, “Geometry-invariant gradient refractive index lens: analytical ray tracing,” *J. Biomed. Opt.*, vol. 17, 2012, Art no. 055001.
[12] C. J. Sheil, and A. V. Goncharov, “Accommodating volume-constant age-dependent optical (AVOCADO) model of the crystalline GRIN lens,” *Biomed. Opt. Express*, vol. 7, pp. 1985–1999, 2016.
[13] R. Navarro, F. Palos, and L. González, “Adaptive model of the gradient index of the human lens. I. Formulation and model of aging ex vivo lenses,” *J. Opt. Soc. Am. A*, vol. 24, pp. 2175–2185, 2007.
[14] Q. Li, and F. Z. Fang, “Physiology-like crystalline lens modelling for children,” *Opt. Express*, vol. 28, pp. 27155–27180, 2020.
[15] K. Ishii, M. Yamanari, H. Iwata, Y. Yasuno, and T. Oshika, “Relationship between changes in crystalline lens shape and axial elongation in young children,” *Invest. Ophthalmol. Vis. Sci.*, vol. 54, pp. 771–777, 2013.
[16] M. Dubbelman, and G. Van der Heijde, “The shape of the aging human lens: curvature, equivalent refractive index and the lens paradox,” *Vision Res.*, vol. 41, pp. 1867–1877, 2001.
[17] E. Martinez-Enriquez, A. de Castro, A. Mohamed, et al., “Age-related changes to the three-dimensional full shape of the isolated human crystalline lens,” *Invest. Ophthalmol. Vis. Sci.*, vol. 61, p. 11, 2020.
[18] A. Khan, J. M. Pope, P. K. Verkicharla, M. Suheimat, and D. A. Atchison, “Change in human lens dimensions, lens refractive index distribution and ciliary body ring diameter with accommodation,” *Biomed. Opt. Express*, vol. 9, pp. 1272–1282, 2018.
[19] E. Kreyszig, *Differential Geometry*, New York, Dover Publications, 1991.
[20] L. N. Thibos, W. Wheeler, and D. Horner, “Power vectors: an application of Fourier analysis to the description and statistical analysis of refractive error,” *Optom. Vis. Sci.*, vol. 74, pp. 367–375, 1997.
[21] G. Dai, *Wavefront Optics for Vision Correction*, Washington, SPIE Press, 2008.
[22] T. Liu, and L. N. Thibos, “Interaction of axial and oblique astigmatism in theoretical and physical eye models,” *J. Opt. Soc. Am. A*, vol. 33, pp. 1723–1734, 2016.
[23] S.-M. Li, N. Wang, Y. Zhou, et al., “Paraxial schematic eye models for 7-and 14-year-old Chinese children,” *Invest. Ophthalmol. Vis. Sci.*, vol. 56, pp. 3577–3583, 2015.
[24] Q. Li, and F. Z. Fang, “Retinal contour modelling to reproduce two-dimensional peripheral spherical equivalent refraction,” *Biomed. Opt. Express*, vol. 12, pp. 3948–3964, 2021.
[25] J. Birkenfeld, A. de Castro, and S. Marcos, “Astigmatism of the ex vivo human lens: surface and gradient refractive index age-dependent contributions,” *Investig. Ophthalmol. Vis. Sci.*, vol. 56, pp. 5067–5073, 2015.